Journal of Physics D: Applied Physics

Tuning defect-related optical bands by channeling implants in semiconductors

To cite this article before publication: Alexander Azarov *et al* 2022 *J. Phys. D: Appl. Phys.* in press https://doi.org/10.1088/1361-6463/aca778

Tuning defect-related optical bands by channeling implants in semiconductors

Alexander Azarov[1,a], Augustinas Galeckas[1], Francis Chi-Chung Ling[2]

and Andrej Kuznetsov[1,a]

[1] *University of Oslo, Centre for Materials Science and Nanotechnology, PO Box 1048 Blindern, N-0316 Oslo, Norway*

[2] *Department of Physics, The University of Hong Kong, Pokfulam, Hong Kong, People's Republic of China*

Ion implantation is an excellent method to introduce defects into semiconductors, extending their functionalities in a controllable way. Herein, we investigated an option to use crystallographically aligned implants as an additional route to control the balance between optically active defects, selecting ZnO as a test material. The optical data were correlated with the structural analysis confirming the formation of different dominating crystalline defects in samples implanted along and off [0001] direction. Specifically, we demonstrated that different proportions in the contents of the extended and point defects in the initial as-implanted states of these samples, lead to prominent variations in the defect-related luminescence upon annealing. As such, we conclude that channeling implants may have an added value in the functionalization of defects in semiconductors, e.g. to tune specific spectral contents in the defect-related emission bands.

Keywords: channeling, photoluminescence, defects, ion implantation

[a)] Authors to whom correspondence should be addressed: alexander.azarov@smn.uio.no, andrej.kuznetsov@fys.uio.no

Introduction

Ion implantation is a powerful tool for material modification and has been one of the primary techniques for semiconductor device processing during the past several decades [1]. In particular, ion bombardment can be used for selective area doping, phase modifications as well as for introducing defects of various types. Moreover, the research on ion-induced defects in semiconductors has recently regained significant interest due to the demands of rapidly developing quantum technologies, where isolated defects with specific properties are the primary building blocks [2]. In this context, extending the possibilities of achieving the desired defect functionalities by means of ion implants is of great interest.

Notably, the channeling effects have been studied in detail along with the host of other parameters determining the quantity and distribution of ion-implantation induced defects in materials [3,4]. Indeed, ions incident along differently dense crystallographic directions will penetrate to different depths even though initially possessing the same energy [5]. Typically, channeling is unwanted as a parasitic effect leading to uncontrollable broadening of the implanted dopant profiles [3-5] and represents one of the key factors limiting the development of the single-ion implantation technology [6,7]. On the other hand, in some cases a broader profile is desirable and such can be realized by a single channeling implant instead of multiple step random implants [8]. Overall, channeling implants can be helpful in providing an extra route for controllable defect engineering [9]. However, to the best of our knowledge, no attempts to interconnect the changes in the defect balance with the optical functionalities in semiconductors subjected to channeling implants have been reported in the literature so far.

In order to investigate such potential correlations we have chosen ZnO as a test semiconductor on behalf of its excellent optical properties [10,11]. Moreover, this system is particularly advantageous for monitoring implantation-induced effects

because of the well-established spectral signatures of the native and radiation defects that collectively comprise a broad deep-level emission (DLE) band [12]. It should also be noted that despite extensive investigation of the radiation phenomena in ZnO [13-17], specific studies on channeling implants in this material are practically missing [18]. Therefore, in the present work, we investigated an option to use crystallographically aligned implants as an additional route to control the balance between optically active defects in ZnO. The optical characterization data were correlated with the structural analysis indicating the formation of different dominating crystalline defects in off-axis and on-axis implanted samples. These findings may be used for engineering and functionalization of defects in semiconductors, e.g., to tune specific spectral contents in broad defect-related emission bands.

Experimental

Hydrothermally grown wurtzite ZnO single crystals (obtained from Mineral Ltd.) were implanted at room temperature with 400 keV $^{69}Ga^{+}$ ions to a dose of 2×10^{15} cm^{-2}. The implantations were carried out either along with [0001] aligned direction (on-axis) or tilted at 7° (off-axis) in order to enhance or reduce channeling, respectively. After implantation, the samples were isochronally annealed for 30 min in air at 500, 700 and 900 °C. The structural quality of the samples was analyzed by Rutherford backscattering/channeling spectrometry (RBS/C) with 1.6 MeV $^{4}He^{+}$ ions incident along the [0001] direction and backscattered into a detector positioned at 165° relative to the incident beam direction. Note that only Zn-related RBS/C data are presented and analyzed in the present study because of the higher sensitivity of the method to heavier atoms (Zn) as compared to light elements (O). The Ga and residual impurity Li concentration *vs* depth profiles in the as-implanted and annealed samples were measured by secondary ion mass spectrometry (SIMS) using a Cameca IMS 7f

microanalyzer with 10 keV O_2^+ ions as the primary beam. The optical properties of the samples were monitored by a steady-state photoluminescence (PL) spectroscopy measurements performed at 10 K using a 325 nm wavelength cw-HeCd laser as an excitation source. Taking into account that the ZnO absorption coefficient is of ~2.5×10^5 cm^{-1} for 325 nm laser excitation [19], the depth range, from which the PL signal was collected, corresponds well to the implanted region.

Results and discussion

The role of channeling on the disorder formation and the shape of the Ga distribution is illustrated by Fig. 1 showing the RBS/C spectra and the corresponding Ga profiles in the samples implanted along and off [0001] direction. For the off-axis Ga implants, the RBS/C spectrum demonstrates a rapid ramp leading to a high dechanneling yield starting from the depth corresponding to the maximum of the Ga depth profile. This profile is shown by the black solid line in Fig. 1 and its position corresponds well with the theoretically predicted projected range (R_p) of the Ga ions of ~140 nm in accordance with the SRIM code [20]. Notably, the high dechanneling yield is maintained behind the ion projected range without any noticeable decrease, in spite of a decreasing number of the primarily defects generated behind R_p. In fact, this effect is known from literature and can be attributed to a high concentration of extended defects in the implanted region acting as strong dechanneling centers [21,22]. In its turn, spatially localized defect structures, such as point defects and defect clusters (both referred to as "point defects" henceforward for simplicity), contribute to the direct backscattering of the analyzing beam determining the disorder magnitude at the projected range depth. Thus, the shape of the RBS/C spectrum in Fig. 1 may indicate that the disorder in the off-axis implanted sample contains a large portion of extended

defects, mixed with point defects, corroborating with the transmission electron microscopy results [23]. Note that despite that exact type of the extended defects as well as the ratio between the point and extended defects is not possible to determine based on the RBS/C data alone, our results unambiguously indicate the complex defect structure containing both types of defects.

For the on-axis implantation, the shape of the Ga profile (red solid line in Fig. 1) is broader with the maximum at ~230 nm as might be expected for channeling. Notably, the dechanneling yield at <300 channels numbers remains high and close to that in the off-axis implanted sample. However, it is important to notice that the disorder formed by the on-axis implantation is significantly lower in the near surface region as compared to that for the off-axis implantation. In other words, already in as-implanted state, the on- and off-axis implanted samples are exhibiting different proportions of the extended and point defects in the region to be probed by PL for further comparison (see below).

The disorder annealing kinetics in the off-axis and on-axis implanted samples is illustrated by Fig. 2 showing the RBS/C spectra of the samples before and after different anneals. Interestingly, for the off-axis implanted samples, the disorder decreased already upon the 500 °C anneal and remains practically unchanged after annealing at 700 °C, as seen from the comparison of the RBS/C spectra in Fig. 2(a). Note that some increase of the dechanneling yield after 700 °C can be attributed to the defect reconstruction during anneals leading to increase of the extended defect fraction in the implanted region. However, more studies are required in order to reveal the exact mechanism of the defect transformation during the medium temperature annealing. Further annealing at 900 °C leads to a recovery of the crystalline lattice and the RBS/C spectrum becomes close to the virgin one. In contrast, more gradual removal of the disorder is observed in the on-axis implanted samples showing a disorder reduction for the 700 °C annealing step too.

The difference in the disorder annealing kinetics in off-axis and on-axis implanted samples can be directly attributed to the thermal stability of the extended and point defects existing in the samples in different proportions, consistently with the data in Fig. 1. It should also be noted that disorder stability and annealing kinetics in ZnO may depend on the implanted species if the defect-dopant reactions are involved in the disorder accumulation [24,25]. Thus, the potential role of the Ga atoms on the defect evolution during post-implantation annealing will be discussed below.

Further insights into the role of channeling on the defect formation in ZnO as well as on the recovery of crystallinity upon thermal annealing can be attained from the PL analysis. Fig. 3 presents side-by-side comparison of the PL spectra of the on-axis and off-axis implanted samples after 500 and 700 °C anneals along with the reference spectrum of the non-implanted (virgin) ZnO sample. The low-temperature PL of ZnO typically comprises two distinct spectral components corresponding to the near-band-edge (NBE) emission and DLE, the intensity ratio of which (NBE/DLE) commonly considered as a measure of crystallinity. Hence, the evolution of NBE/DLE allows for monitoring the crystallinity changes during the processing. The virgin sample exhibits PL features typical to high-quality ZnO crystal, i.e., very high luminescence yield (intensity scaled by a factor of 0.01 in Fig. 3) with the excitonic NBE emission dominating by two orders of magnitude over the defect-related DLE band. The implantation-induced disorder introduces non-radiative pathways that dramatically suppress PL in the as-implanted samples (not shown), whereas the subsequent post-annealing leads to general increase of the luminescence yield signifying the lattice recovery [26]. While monitoring NBE allows for evaluating recovery of the crystallinity, the DLE exposes the dominating defects along with their developments upon ion-implantation and post-anneals. Indeed, the broad DLE band is actually comprised of two emission components conventionally labeled as red luminance (RL)

centered at ~1.8 eV and green luminescence (GL) at ~2.5 eV, respectively. The RL component is usually attributed to the open volume defects such as zinc vacancy clusters [27], while the assignment of GL remains unsettled with an isolated zinc vacancy being a prime candidate [28].

As seen from Fig. 3, the NBE and DLE features re-emerge upon 500 °C anneals in both on-axis and off-axis implanted samples. The NBE intensity remains nearly the same in both on-axis and off-axis implanted samples implying comparable levels of the residual crystalline disorder. By contrast, the DLE intensity and its spectral content differ significantly demonstrating enhanced (by an order of magnitude) RL for the on-axis implanted sample, while GL magnitude remains similar in both samples. Despite the distinct difference between the ratio of RL/GL spectral components in the off- and on-axis implanted samples, an unambiguous interpretation of the PL results is not straightforward. Indeed, in accordance with the literature reports [10-12, 27-28], the observed RL increase can be attributed to a higher concentration of open volume defects in the on-axis implanted samples as compared to that for the off-axis implants. The observed difference can be also explained by the prevalence of non-radiative recombination pathways in the off-axis implanted samples. However, this mechanism should lead to the overall decrease of the PL yield, rather than to the changes of the spectral component balance.

Further annealings at 700 °C and 900 °C lead to substantial enhancement (by two orders of magnitude) of the total luminescence yield as well as to a change in the RL/GL balance in the samples. Indeed, as seen from Fig. 3, the GL component dominates in the DLE band for both on-axis and off-axis implanted samples. It is noteworthy that PL spectra of the 700 °C annealed samples appear identical in shape, however, the total PL yields are notably different implying certain distinction of the

non-radiative recombination pathways in the off- and on-axis implanted samples. The latter assumption is correlating well with the different residual crystal disorder levels as concluded from the data in Fig. 2. Also noteworthy is the fact that 900ºC anneal is insufficient to fully recover the optical properties of the implanted samples corroborating with the previous results [26].

It should be noted that implanted species can affect the RL/GL balance as it was shown for implants with different rare earth ions [29]. It was demonstrated previously that Ga impurity introduces a donor-bound exciton line in the NBE region [30] and do not contribute to the DLE spectral region directly. However, the Ga atoms can still affect the optical properties of the annealed samples in the DLE range due to their electronic action and interaction with different defects. Thus, we measured the Ga concentration versus depth profiles in the off- and on-axis implanted samples after different anneals as shown in Fig. 4 (a) and (b), respectively. It is seen that there is practically no difference in the Ga behavior in the off- and on-axis implanted samples. Indeed, the implanted Ga atoms are stable up to 700 °C, while the pronounced Ga diffusion is observed in the both samples after 900 °C. The shape of the 900 °C Ga profiles indicates a concentration dependent Ga migration mechanism, where a double negatively charged Zn vacancy is the main mediating defect of Ga diffusion [31]. However, the change in the Fermi level position due to donor action of Ga atoms may affect the formation energy of point defects and, in particular, Zn vacancies [28,32].

Note that incorporation of Ga atoms into the lattice occurs at the temperatures well below 900 °C as can be indirectly traced from the behavior of Li atoms. Thus, in addition to Ga profiles, we have measured the Li ones since the behavior of residual impurity Li during post- implantation annealing in ZnO can be efficiently used to reveal a sublattice localization of the implanted impurity [33]. It is seen that Li exhibits similar

behavior in the off- and on-axis implanted samples. Indeed, after the 500 °C anneals the Li content in the both samples is uniform at the level of ~2×10^{17} cm^{-3} corresponding well to the Li content in the as-grown ZnO samples. However, after 700 °C the Li pushed out the implanted area forming a large depletion region in the both ZnO samples. Such Li behavior is attributed to the strong interaction of substitutional Li with the fast diffusing Zn interstitials formed due to preferential incorporation of Ga atoms on to the Zn sites [33]. Finally, after 900 °C anneals the Li atoms diffuse back and accumulated in the Ga-rich region via trapping at the open volume defects such as Zn vacancies which formation energy can be drastically reduced in this area as mentioned before.

Conclusion

In conclusion, we investigated an option to use crystallographically aligned implants as an additional route to control the balance between optically active defects in semiconductors. The optical data were correlated with the structural analysis confirming the formation of different dominating crystalline defects in off-axis and on-axis implanted ZnO. Specifically, we demonstrated that different proportions in the contents of the extended and point defects in the initial as-implanted states lead to variations of the defect-related luminescence upon annealing. As such, we conclude that channeling implants may have an added value in the functionalization of defects in semiconductors, e.g. to tune specific spectral contents in the defect-related emission bands.

ACKNOWLEDGMENTS

The Research Council of Norway is acknowledged for the support to the Norwegian Micro- and Nano-Fabrication Facility, NorFab, project number 295864. The international collaboration was enabled through the INTPART Program at the Research Council of Norway (projects No. 261574 and No. 322382).

DATA AVAILABILITY STATEMENT

Any data that support the findings of this study are included within the article.

1. Fair R B 1998 History of some early developments in ion-implantation technology leading to silicon transistor manufacturing *Proceedings of the IEEE* **86** 111

2. Maurer P C, Kucsko G, Latta C, Jiang L, Yao N Y, Bennett S D, Pastawski F, Hunger D, Chisholm N, Markham M, Twitchen D J, Cirac J I and Lukin M D 2012 Room-temperature quantum bit memory exceeding one second *Science* **336** 1283

3. Robinson M T 1994 Basic physics of radiation damage production *J. Nucl. Materials* **216** 1

4. Raineri V, Privitera V, Galvagno G, Priolo F and Rimini E 1994 Channeling implants in silicon crystals *Mat. Chem. and Phys.* **38** 105

5. Nordlund K, Djurabekova F and Hobler G 2016 Large fraction of crystal directions leads to ion channeling *Phys. Rev. B* **94** 214109

6. Cassidy N, Blenkinsopp P, Brown I, Curry R J, Murdin B N, Webb R and Cox D 2021 Single ion implantation of bismuth *Phys. Status Solidi A* **218** 2000232

7. Raatz N, Scheuner C, Pezzagna S and Meijer J 2019 Investigation of ion channeling and scattering for single-ion implantation with high spatial resolution *Phys. Status Solidi A* **216** 1900528

8. Morvan E, Godignon P, Vellvehi M, Hallén A, Linnarsson M and Kuznetsov A Yu 1999 Channeling implantations of Al^+ into 6H silicon carbide *Appl. Phys. Lett.* **74** 3990

9. Pipeleers B, Hogg S M and Vantomme A 2005 Defect accumulation during channeled erbium implantation into GaN *J. Appl. Phys.* **98** 123504

10. Lv J, Li C and Chai Z 2019 Defect luminescence and its mediated physical properties in ZnO *J. of Luminescence* **208** 225

11. Reshchikov M A, Xie J Q, Hertog B and Osinsky A 2008 Yellow luminescence in ZnO layers grown on sapphire *J. Appl. Phys.* **103** 103514

12. Børseth T Moe, Svensson B G, Kuznetsov A Yu, Klason P, Zhao Q X, and Willander M 2006 Identification of oxygen and zinc vacancy optical signals in ZnO *Appl. Phys. Lett.* **89** 262112

13. Turos A, Jóźwik P, Wójcik M, Gaca J, Ratajczak R and Stonert A 2017 Mechanism of damage buildup in ion bombarded ZnO *Acta Mater.* **134** 249

14. Azarov A Yu, Wendler E, Kuznetsov A Yu and Svensson B G 2014 Crucial role of implanted atoms on dynamic defect annealing in ZnO *Appl. Phys. Lett.* **104** 052101

15. Kucheyev S O, Williams J S, Jagadish C, Zou J, Evans C, Nelson A J and Hamza A V 2003 Ion-beam-produced structural defects in ZnO *Phys. Rev. B* **67** 094115

16. Lorenz K, Alves E, Wendler E, Bilani O, Wesch W and Hayes M 2005 Damage formation and annealing at low temperatures in ion implanted ZnO *Appl. Phys. Lett.* **87** 191904

17. Kennedy J, Murmu P P, Manikandan E and Lee S Y 2014 Investigation of structural and photoluminescence properties of gas and metal ions doped zinc oxide single crystals *J. Alloys and Comp.* **616** 614

18. Rita E, Alves E, Wahl U, Correia J G, Monteiro T, Soares M J, Neves A and Peres M 2006 Stability and luminescence studies of Tm and Er implanted ZnO single crystals *Nucl. Instrum. Methods Phys. Res. B* **242** 580

19. Gadallah A-S and El-Nahass M M 2013 Structural, optical constants and photoluminescence of ZnO thin films grown by sol-gel spin coating *Adv. in Cond. Matter Phys.* 234546

20. Ziegler J F, Ziegler M D and Biersack J P 2010 SRIM – The stopping and range of ions in matter (2010) *Nucl. Instrum. Methods Phys. Res. B* **268** 1818

21. Turos A, Nowicki L, Stonert A, Pagowska K, Jagielski J and Muecklich A 2010 Monte Carlo simulations of ion channeling in crystals containing extended defects *Nucl. Instrum. Methods Phys. Res. B* **268**, 1718

22. Wendler E, Bilani O, Gärtner K, Wesch W, Hayes M, Auret F D, Lorenz K and Alves E 2009 Radiation damage in ZnO ion implanted at 15 K *Nucl. Instrum. Methods Phys. Res. B* **267** 2708

23. Perillat-Merceroz G, Gergaud P, Marotel P, Brochen S, Jouneau P-H and Feuillet G 2011 Formation and annealing of dislocation loops induced by nitrogen implantation of ZnO *J. Appl. Phys.* **109** 023513

24. Sonder E, Zhur R A and Valiga R E 1988 Annealing of damage and stability of implanted ions in ZnO crystals *J. Appl. Phys.* **64** 1140

25. Azarov A Yu, Svensson B G and Kuznetsov A Yu 2012 Impurity-limited lattice disorder recovery in ion-implanted ZnO *App. Phys. Lett.* **101** 222109

26. Azarov A, Galeckas A, Mieszczyński C, Hallén A and Kuznetsov A 2020 Effects of annealing on photoluminescence and defect interplay in ZnO bombarded by heavy ions: Crucial role of the ion dose *J. Appl. Phys.* **127** 025701

27. Knutsen K E, Galeckas A, Zubiaga A, Tuomisto F, Farlow G C, Svensson B G and Kuznetsov A Yu 2012 Zinc vacancy and oxygen interstitial in ZnO revealed by sequential annealing and electron irradiation *Phys. Rev. B* **86** 121203(R)

28. Janotti A and Van de Walle C G 2007 Native point defects in ZnO *Phys. Rev. B* **76** 165202

29. Ratajczak R, Guziewicz E, Prucnal S, Łuka G, Böttger R, Heller R, Mieszczynski C, Wozniak W and Turos A 2018 Luminescence in the visible

region from annealed thin ALD-ZnO films implanted with different rare earth ions *Phys Status Solidi A* 1700889

30. Meyer B K, Alves H, Hofmann D M, Kriegseis W, Forster D, Bertram F, Christen J, Hoffmann A, Straßburg M, Dworzak M, Haboeck U and Rodina A V 2004 Bound exciton and donor–acceptor pair recombinations in ZnO *Phys. Status Solidi B* **241** 231

31. Sky T N, Johansen K M, Riise H N, Svensson B G and Vines L. 2018 Gallium diffusion in zinc oxide via the paired dopant-vacancy mechanism *J. Appl. Phys.* **123** 055701

32. Azarov A, Venkatachalapathy V, Mei Z, Liu L, Du X, Galeckas A, Monakhov E, Svensson B G and Kuznetsov A 2016 Self-diffusion measurements in isotopic heterostructures of undoped and *in situ* doped ZnO: Zinc vacancy energetics *Phys. Rev B* **94** 195208

33. Azarov A Yu, Knutsen K E, Neuvonen P T, Vines L, Svensson B G and Kuznetsov A Yu 2013 Impurity sublattice localization in ZnO revealed by Li marker diffusion *Phys. Rev. Lett.* **110** 175503

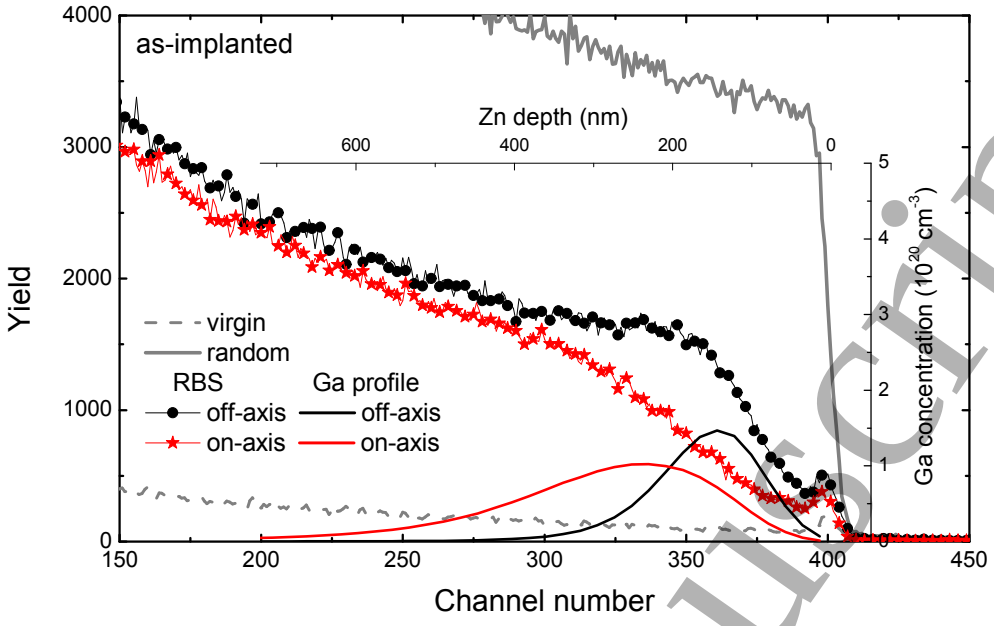

Fig. 1 RBS/C and corresponding Ga profiles, as measured by SIMS, of ZnO samples implanted with 400 keV Ga ions to 2×10^{15} cm^{-2} at random (off-axis) and aligned (on-axis) directions. The channeling spectrum of unimplanted (virgin) sample is shown for comparison by the dashed line.

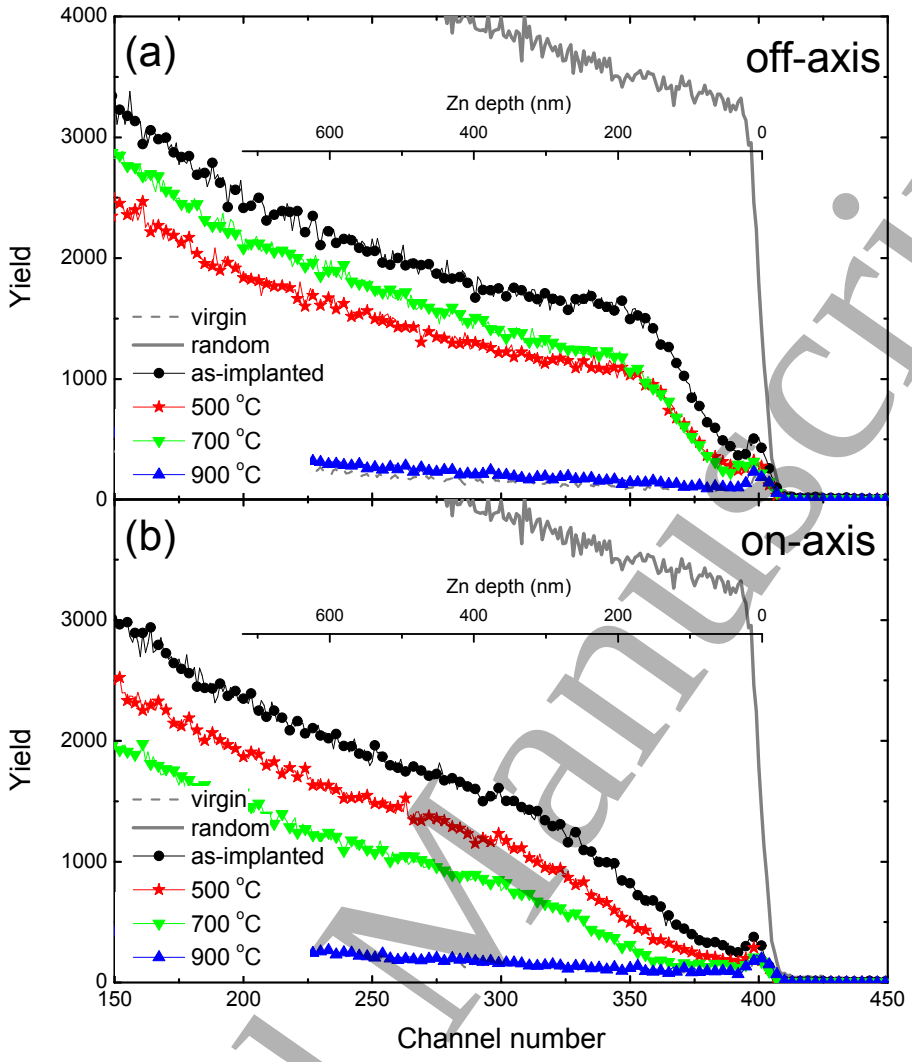

Fig. 2 RBS/C spectra of ZnO samples implanted with 400 keV Ga ions to 2×10^{15} cm^{-2} at (a) random (off-axis) and (b) aligned (on-axis) directions before and after annealing at different temperatures as indicated in the legends. The channeling spectra of unimplanted (virgin) sample are shown for comparison by the dashed lines in both panels.

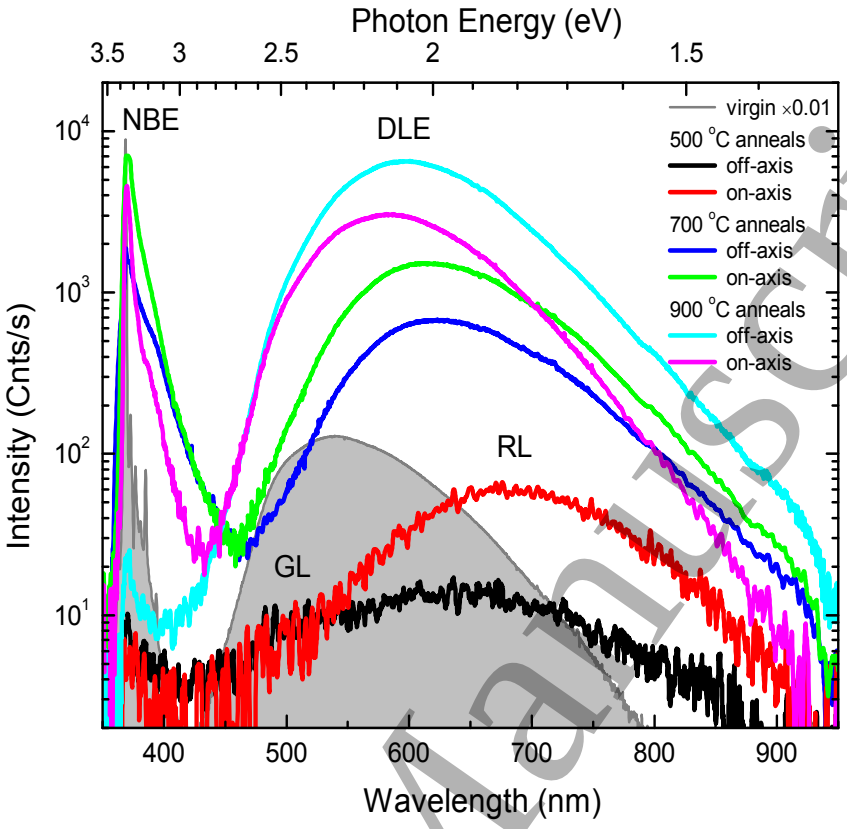

Fig. 3 PL spectra obtained at 10 K of the samples implanted with on-axis and off-axis Ga ions after different anneals as indicated in the legend. The PL spectrum of unimplanted (virgin) sample is shown for comparison (scaled by a factor of 0.01). The RL and GL bands within the multi-component structure of DLE are indicated for clarity.

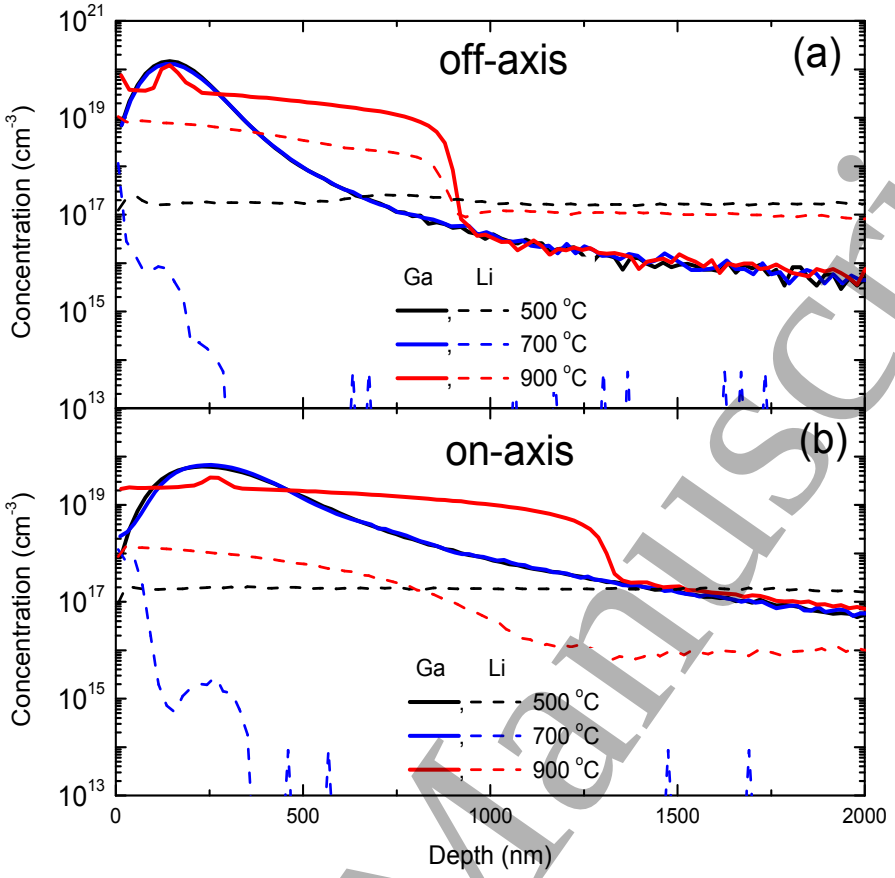

Fig. 4 Ga concentration versus depth profiles (solid lines) and corresponding Li ones (dashed lines) in the (a) off- and (b) on-axis implanted samples after different anneals as indicated in the legends.